Study of the rheological properties of water and Martian soil simulant mixtures for engineering applications on the red planet

Taylor, Lewis; Alberini, Federico; Sullo, Antonio; Meyer, Marit E.; Alexiadis, Alessio

DOI:
10.1016/j.asr.2017.12.037

Document Version
Peer reviewed version

Citation for published version (Harvard):
Taylor, L, Alberini, F, Sullo, A, Meyer, ME & Alexiadis, A 2018, 'Study of the rheological properties of water and Martian soil simulant mixtures for engineering applications on the red planet', *Advances in Space Research*. https://doi.org/10.1016/j.asr.2017.12.037

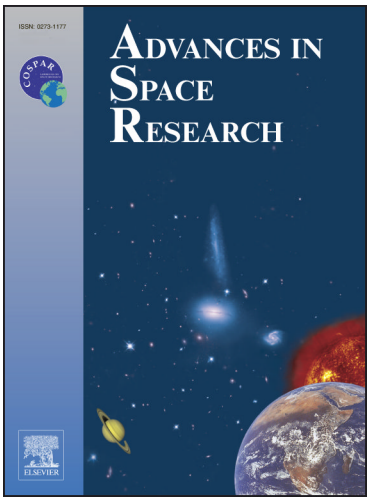

Study of the rheological properties of water and Martian soil simulant mixtures for engineering applications on the red planet

Lewis Taylor, Federico Alberini, Antonio Sullo, Marit E. Meyer, Alessio Alexiadis

PII: S0273-1177(18)30004-8
DOI: https://doi.org/10.1016/j.asr.2017.12.037
Reference: JASR 13570

To appear in: *Advances in Space Research*

Received Date: 12 September 2017
Revised Date: 14 December 2017
Accepted Date: 27 December 2017

Please cite this article as: Taylor, L., Alberini, F., Sullo, A., Meyer, M.E., Alexiadis, A., Study of the rheological properties of water and Martian soil simulant mixtures for engineering applications on the red planet, *Advances in Space Research* (2018), doi: https://doi.org/10.1016/j.asr.2017.12.037

Study of the rheological properties of water and Martian soil simulant mixtures for engineering applications on the red planet.

Lewis Taylor[a], Federico Alberini[a], Antonio Sullo[b], Marit E. Meyer[c], Alessio Alexiadis[a*]

[a]School of Chemical Engineering, University of Birmingham, Birmingham B15 2TT United Kingdom.

[b]Diageo, Dunmow Rd, Birchanger, Bishop's Stortford CM23 5RG, United Kingdom.

[c]NASA Glenn Research Center, Cleveland, Ohio 44135 United States of America.

Abstract

The rheological properties of mixtures of water and the Martian soil simulant *JSC-Mars-1A* are investigated by preparing and testing samples at various solids concentrations. The results indicate that the dispersion is viscoelastic and, at small timescales (~0.1 s), reacts to sudden strain as an elastic solid. At longer timescales the dispersion behaves like a Bingham fluid and exhibits a yield stress. Hysteresis loops show that rapid step-changes (2 s duration) of shear-rate result in thixotropic behaviour, but slower changes (>10 s duration) can result in rheopexy. These observations are explained with the breakdown and recovery of the packing structure under stress. The rheological information is used to generate practical tools, such as the system curve and the Moody chart that can be used for designing piping systems, and calculating pump sizes and pressure requirements.

Keywords: Rheology; Thixotropy; Solid dispersion; Martian regolith simulant; In situ resource utilization (ISRU).

1. Introduction

As humans look towards the future of space exploration, the question of becoming a multi-planetary species emerges. This feat will require extensive technology development in order to create habitats that can sustain human life. One of the barriers to long term space exploration is the enormous expense and difficulty of transporting mass out of Earth's gravity well. In order to minimize the mass

transported from Earth during these missions, the utilization of local resources (known as in situ resource utilization) must therefore be maximized. In this context, building materials deserve special attention since they are intrinsically heavy and usually required in large quantities.

A promising solution involves utilising local regolith for the production of construction material. A number of studies focus on the production of cementitious materials from Lunar regolith simulants (e.g. Happel et al., 1993; Cesaretti et al., 2014; Montes et al., 2014; Alexiadis et al., 2017) or Martian regolith simulants (e.g. Mukbaniani et al., 2015; Lin al., 2016; Alexiadis et al., 2017). In the case of the Martian simulant in particular, alkaline suspensions of the JSC Mars-1A simulant are known to form aluminosilicate gels that, upon curing, result in a hard solid with a compressive strength comparable to that of normal construction bricks.

However, the actual production of these materials necessitates handling the regolith in slurry or paste form, and so the rheology of water-regolith dispersions must be understood for optimal design of associated transport and process equipment such as pipes, pumps and mixers. Additionally, 3D printing is the latest trend in the construction industry and it has been proposed for constructing off-Earth habitats (Leach et al., 2012; Cesaretti et al., 2014). A good understanding of the rheology is paramount also in this case. The fresh geopolymer must be extruded smoothly and each bead must hold its shape during the printing process. Moreover, the bead should also hold its shape when another bead is printed on top of it.

The behaviour of solid-liquid dispersions, especially when the solid phase is present in high concentrations, can be quite complex and includes occurrences such as shear-history dependent rheology (e.g. thixotropy or rheopexy), stick-slip, non-uniform packing distribution, and other phenomena, which have been collectively defined as *granulo-viscous* phenomena (Cheng and Richmond, 1978).

In this work, we study the properties of dispersions of water with the Martian dust simulant JSC Mars-1A. In particular, we focus on (i) the extent and timescales of history-dependent phenomena over a range of solids contents and shear rates, (ii) the existence of other time-dependent

influences on viscosity (i.e. ageing), and (iii) characterise the underlying slurry rheology over a range of solids contents. As a high pH induces geopolymerization, a preliminary investigation into the rheology of an alkaline suspension is also undertaken.

These data are then converted into the *system curve* and the *Moody chart* of the fluid, which can be used to optimise the design and operation of slurry handling equipment.

2. Materials and methods

This section is organized as follows. Section 2.1 describes the preparation and composition of the samples used in rheological testing. Since geopolymerization of JSC-Mars-1A requires milling to reduce the particle size, all the rheological tests were carried out with milled simulant; the size distribution after milling is shown in Section 2.2, while the methodology of the rheological tests performed are described in Section 2.3.

2.1 Samples

The Martian simulant used is *JSC-Mars-1A* (Orbitec, USA). It is mined from the Pu'u Nene cinder cone in Hawaii, and was designed to be a spectral analogue of the 'bright regions' of Mars. The elemental oxide composition of the simulant as measured by Allen et al., 1998 is shown in Table 1 and is compared to a typical Martian regolith composition (Taylor and McLennan, 2008). During this study, the simulant was first milled, and then water was added to form a suspension. The standard procedure used for rheological testing required that these samples were tested shortly after preparation. However, some samples were tested after a number of days of exposure to water, to study ageing effects as discussed in Section 4.4. The samples used in the experiments are reported in Table 2. The concentration range was chosen on the basis of our previous work on geopolymerization (Alexiadis et al., 2017). For the geopolymer experiments (Section 4.5), sodium hydroxide pellets were dissolved into the $\phi = 0.39$ sample to form an 8M NaOH suspension.

2.2 Milling

A *Pulverisette 5* planetary ball mill (Fritsch, Germany) was used for comminution. For each grind, 100 g of powder was loaded into a 250 mL grinding vessel with 500 g of 3 mm stainless steel media. The grind was run at 200 rpm for 30 minutes. This was repeated until around 700 g of dust was acquired, which was subsequently mixed together. The particle size distribution of this mixture was measured using a *Malvern Mastersizer 2000* laser diffraction particle size analyser (Malvern Instruments, UK), the results of which are shown for both the unground and ground simulant in Fig. 1a (d_{50} = 10 . 1 µm). Fig. 1b shows a representative SEM image of the milled regolith.

2.3 Rheological measurements

An AR-G2 rheometer (TA Instruments) was used for rheological testing. A vane spindle geometry was used since it mitigates jamming from large particles, and wall slip in yield stress fluids is less problematic than in other geometries (Barnes and Nguyen, 2001; Saak et al., 2001). A number of alternative tests were carried out with both parallel-plate and cone-and-plate geometries, but results were not reproducible as for the vane spindle and, therefore, disregarded.

The vane spindle has a height of 42mm and a radius of 14mm. The stator inner radius is 15mm, and the clearance from the bottom of the pot was 4mm. A water bath maintained the temperature at 20°C.

During rheological testing, enough sample was placed in the pot to completely submerge the spindle head. The rheometer was used to carry out hysteresis loop tests, step tests and oscillatory tests.

2.3.1 Hysteresis loop tests

The hysteresis loop curves in Section 4.1 were produced by applying a series of shear rate step increases up to a maximum shear rate, and recording the resulting shear stress at the end of each step, to produce an ‘up-curve’. This is followed by a series of equivalent shear rate step decreases, producing a ‘down-curve’. In some cases, several consecutive iterations need to be carried out to obtain an ‘equilibrium’ hysteresis loop (Ovarlez, 2011). The shear rate was varied between 1/s and 100/s, and each up-curve and down-curve consisted of 10 consecutive steps. The duration for which each step was held was changed between experimental runs, and took values of 30 s, 10 s, and 2 s.

The following procedure was used:

1. The sample was rested for 5 minutes at the beginning of each cycle.
2. A step duration (30, 10, or 2 s) is selected, and the first up-curve is run, followed by the down-curve.
3. Immediately after the down-curve, the next hysteresis cycle is run.
4. Step 3 is repeated at least until an 'equilibrium' hysteresis loop curve is reached (i.e. there is little change from the previous loop, usually achieved after the 2nd iteration).
5. Steps 1-4 are repeated at the next step duration value.

2.3.2 Step tests

For the step tests in Section 4.1, the following procedure was used:

1. Pre-shear from rest at 5/s, for 300 s
2. A shear rate step change to 10/s, 20/s, 40/s, 70/s or 100/s is applied for 150 s.
3. Shear rate is reduced back to 5/s, and held for 150 s.
4. Without allowing the fluid to rest, Step 2-3 is repeated with a different shear rate step.
5. The shear rate chosen increases with iteration, and resets after 100/s back to 10/s. The above sequence is carried out until at least three data points for each shear rate step are obtained.

2.3.3 Oscillation tests

The following procedure was used for oscillatory testing in Sections 4.2:

1. After preparation, the sample is rested for 5 minutes.
2. A strain sweep was carried out, where the vane oscillated at a frequency of 1 Hz, and the % strain was varied on a logarithmic scale between 1 x 10^{-4} and 100.
3. The sample was rested again for 5 minutes.

4. Frequency sweeps, where the strain % was set within the linear viscoelastic region identified within the strain sweep, were carried out with the frequency varied between logarithmic decades of 0.01 and 100 Hz.

3. Dimensional analysis

The viscosity of a solid-liquid suspension can be expressed, in general, as a function of various parameters (Stickel et al., 2005).

$$\eta = f(d, \rho_P, n, \eta_0, \rho_0, kT, \dot{\gamma}, t) \quad (1)$$

where d is the particle size, ρ_p the particle density, n the particle concentration, η_0 the liquid viscosity, ρ_0 the liquid density, kT the thermal energy, $\dot{\gamma}$ the shear rate, and t the time. For the moment, we assume monodispersed particles and ignore the particle size distribution. According to the Buckingham π theorem, the number of variables can be reduced from nine to six.

$$\eta_r = f(\rho_r, \phi, De, Pe, Ba) \quad (2)$$

where

$$\eta_r = {}^{\eta}/_{\eta_0} \quad (3)$$

is the relative viscosity,

$$\rho_r = {}^{\rho_P}/_{\rho_0} \quad (4)$$

the relative density,

$$\phi = n\frac{\pi}{6}d^3 \quad (5)$$

the volume fraction,

$$De = {}^{t_c}/_{t} \quad (6)$$

the Deborah number, where t_c is the stress relaxation time,

$$Pe = \frac{6\pi\eta_0 d^3\dot{\gamma}}{kT} \tag{7}$$

the Peclet number, and

$$Ba = \frac{\rho_P \lambda^{1/2} d^2\dot{\gamma}}{\eta_0} \tag{8}$$

the Bagnold number, where λ is the linear concentration defined by

$$\lambda = \frac{1}{(\phi_m/\phi)^{1/3}-1} \tag{9}$$

Where ϕ_m is the maximum possible solids volume fraction. Instead of Ba, rheologists often use the Reynolds number Re defined in a similar form to Ba in Eq. (8), but neglecting the λ term. In this work we prefer Ba, which is used in granular mechanics, because, unlike Re, it explicitly accounts for the concentration ϕ. This is useful later on when discussing Fig. 2. The *granular regime*, for instance, could not be accounted for in Fig. 2, if Re instead of Ba is used.

If the system is neutrally buoyant ($\rho_r \sim 1$) and at steady-state (De→0), Eq. (2) can be further simplified to

$$\eta_r = f(\phi, Pe, Ba) \tag{10}$$

The effect of Pe and Ba (or Re) is often divided into separate intervals that define various rheological regimes as indicated in Fig. 2; for details on how to derive Fig.2 at low Ba, where Ba is qualitatively analogous to Re, see (Ovarlez, 2011); for details on how to derive Fig. 2 at higher Ba see (Stickel et al., 2005).

Within each region of Fig. 2, the rheology only depends on the solids volume fraction, and so Eq. (10) is reduced to

$$\eta_r = f(\phi) \tag{11}$$

This division of the Pe-Ba plane in separated regions provides a useful reference, but it is somewhat arbitrary, and often differs from study to study (e.g. Schramm, 1994; Duran, 2000; Stickel et al., 2005;

Kawasaki et al., 2014). Moreover, it refers to monodisperse suspensions, while in practice suspensions are almost always polydisperse. If we calculate different values of Pe and Ba for each size *d* of the particle-size distribution in Fig. 1, we obtain the grey area in Fig. 2. Therefore, under certain conditions, the dispersion can cover several regions at the same time: the smallest particles (~1 μm), for instance, can be in the shear thinning region, the intermediate particles (~10 μm) in the Newtonian region and the largest (~100 μm) in the shear thickening region. This does not mean that the rheology will simply be a combination of these three behaviours; overall Fig. 2 is not indicative of polydisperse suspensions and complex interactions among particles of different size are expected in polydisperse solutions. In the following section, some observations of the complex rheological behaviour occurring in the milled JSC Mars 1A simulant suspensions are discussed.

4. Results and discussion

This section is organized as follows: initially, the hysteresis loops for water-simulant dispersions at different concentrations are presented and their major features highlighted. Subsequently, the data for each sample are fitted to the Bingham model to determine τ_Y (yield stress) and η (viscosity). In Section 4.3, the effect of solids volume fraction on τ_Y and η is discussed. Ageing also affects the rheology of the samples and this is discussed in Section 4.4. In Section 4.5, the effect of a high pH, which is necessary to start the process of geopolymerization, is examined.

4.1 Hysteresis loops and step tests

Ten linear steps increments from 1 s^{-1} to 100 s^{-1} were carried out for the up-ramp, followed by the same steps in reverse order to form the down-ramp with the procedure described in Section 2.3.1. Three different step durations (2 s, 10 s or 30 s) were implemented in order to study the response of the dispersion to changes of different characteristic times. For every sample, multiple hysteresis loop series were carried out, each consisting of several consecutive loops, with 5 minutes rest in between each series. The first loop is usually different from the others and a reproducible steady-state profile is only found after a few repetitions. A typical result is shown in Fig. 3 where the hysteresis between the first up-curve and first down-curve is substantial. Subsequent loops show a decrease of hysteresis and

equilibrium is reached after two or three cycles. The shape of the first loop can change if the same experiment is repeated with a new sample and it depends on how the sample has been mixed during its preparation and how long it has been at rest. The steady-state loops, on the other hand, remain constant and, for this reason, the following discussion is based only on the steady-state profiles.

Fig. 4 compares different step durations between a relatively low concentration ($\phi = 0.44$) and a high concentration ($\phi = 0.49$) dispersion. At a shear rate of around 10 s^{-1}, a 'spike' in shear stress appears at both high and low concentrations. This phenomenon is relatively common in densely loaded suspensions and it has been described in previous studies (e.g. Cheng and Richmond, 1978; Cheng, 1984; Chappuis and Guinot 1992; Fall et al., 2008; Brown and Jaeger, 2012). It is attributed to the transition between low-shear and a high-shear packing distributions. For the transition to occur, the structure must temporarily dilate to allow for the relative motion of the particles rearranging from the old to the new packing and causing the spike-like shear stress increment observed in Fig. 4 (Duran, 2000; Wegner and Brady 2009).

The area within the hysteresis loop measures the extent of thixotropy and its prominence depends on both solids concentration and step duration. At low concentrations, the hysteresis gradually disappears with increasing shear duration (compare Fig. 4a, 4b and 4c). This is expected, since long shear times can cause complete relaxation of the sample.

At high concentrations however, the behaviour changes from thixotropic to rheopectic as the step duration increases (compare Fig. 4d to Fig. 4e and 4f). This behaviour has been observed in other cases (e.g. Cheng and Richmond, 1978; Fall et al., 2008; Brown and Jaeger, 2012; Wegner and Brady 2009; Cheng et al., 2011) and are generally believed to arise due to jamming and release of particles associated with the non-uniform formation of temporary mesoscopic agglomerates or, in other words, the time scale difference between destruction and reconstruction of internal structure (Cheng 1984; Ness et Sun, 2016). Another possible explanation of the insurgence of rheopexy can be associated with settling (Schramm, 2014), but, as discussed in Section 5.2, settling is not the most likely explanation in this case.

4.2 Rheological models

In this section, we look for a simple rheology model to fit the data. The goal is not to provide the most accurate model possible for fitting the data, but to derive a set of reference values that can be used in Section 4.3 to study the effect of solids volume fraction on the dispersion properties. The effect of thixotropy is considered separately, and the models are fitted to the down-curve (10 s step duration), which is usually smoother and produces a better fitting than the up-curve.

The simplest model that accurately fits the data is the Bingham model

$$\tau = \tau_Y + \eta\dot{\gamma} \tag{12}$$

where τ_Y is the yield stress and η the Bingham viscosity. The fitting yield stress (τ_Y) is not the lowest measured stress of the dispersion (τ^*_Y, at a shear rate of 1 s^{-1}). The difference between the two is illustrated in Fig. 5a and, in general, we observe that $\tau_Y > \tau^*_Y$ for high solids samples.

The concept of yield stress has been questioned since it is often observed that the value depends on the way it is measured (Barnes and Walters, 1985). In particular, experiments at very small shear rates (e.g. 10^{-6} s^{-1}), show a continuous decrease of the yield stress that suggests it may vanish completely at zero shear. Moreover, the response of the dispersion to low shear rates is often related with its viscoelastic properties. To assess these properties in relation to the yield stress, we performed a series of strain sweep oscillation tests at 1 Hz to determine both the elastic modulus (*G'*) and viscous modulus (*G"*) of the suspension. The material behaves as an elastic solid up to a critical strain γ_c (Fig. 5b); at strains higher than γ_c, it becomes increasingly more fluid-like; and, finally, when *G"*> *G'*, viscous fluid behaviour dominates. Fig. 5b also allows estimating the yield stress in relation to the viscoelasticity of the material. This value is generally lower than both τ_Y and τ^*_Y since it refers to higher Deborah numbers.

Despite the above considerations, the yield stress is a practical tool when comparing the rheology of two dispersions. For this reason, in the next section we calculate τ_Y for all the samples based on the Bingham model and use it to assess the effect of ϕ on the rheology.

4.3. Effect of concentration

The fitting parameters τ_Y and η are calculated for all concentrations as discussed in the previous section. We also compare the thixotropic properties of the different dispersions. In order to quantify thixotropy, we measure the hysteresis area α defined as

$$\alpha = \int_{up} \tau d\dot{\gamma} - \int_{down} \tau d\dot{\gamma} \quad (13)$$

where negative values of α indicate rheopexy. Table 3 compares the values τ_Y, η and α for all the solids volume fractions investigated.

As expected, both the yield stress and viscosity increase with concentration, while α changes from thixotropic to rheopectic as discussed in Section 4.1. Fig. 6a displays this behaviour for τ_Y and α, with the changes becoming much more pronounced at higher solids volume fractions.

In the literature, the effect of concentration is often characterised by a maximum volume fraction ϕ_m. Physically, ϕ_m should be the maximum packing fraction for a given suspension, but in practice it is often used as an adjustable parameter in viscosity models.

Quemada (Quemada, 1985), in particular, proposed the following expression, which is derived for particle clustering.

$$\eta_r = \left(1 - \frac{\phi}{\phi_m}\right)^{-q} \quad (14)$$

The theoretical value of q for monodisperse suspension is 2. For polydisperse suspension, q must be determined from the data and usually is larger than 2. Fig. 6b shows that a good fitting can be obtained with $\phi_m = 0.65$ and $q = 3.95$. The maximum theoretical packing for a monodisperse suspension is $\phi_m = 0.64$, but this value can be higher for polydisperse suspensions, as in our case.

4.4 Ageing

In this section, we assess the effect of ageing on yield stress and viscosity. In the samples tested a number of days after their preparation, we observed that the rheological properties changed. The change is not due to evaporation since, by weighing the samples, we verified that no loss of water occurred. The $\phi = 0.44$ sample was chosen to investigate ageing because of its low thixotropy. Several samples were prepared and tested on different days, covering a full week. As shown in Fig. 7, ageing especially affects the yield stress. The milling process is the likely responsible for this behaviour. Milling usually activates the surface of particulate materials (Saak et al., 2001) and the ageing behaviour may be caused by the stabilization of the milled surface of the particulate material. Moreover, the effect of ageing is limited in time: we monitored both the yield stress and the viscosity for a week (Fig. 7) and did not observe any further change after the first three days. This seems consistent with the stabilization hypothesis: after three days, the surfaces are stabilized and further changes do not occur.

4.5 Water-dust mixtures with NaOH

In this section, we investigate the change in rheology when NaOH is added to the dispersion. The experiments were performed at the typical geopolymerization conditions for the Martian simulant (Alexiadis et al. 2017): a NaOH concentration of 8M, and $\phi = 0.39$.

Several thixogram and hysteresis loop tests were carried out. The thixograms show a negligible degree of thixotropicity compared to the case without NaOH. In the shear rate range investigated, the best fit is achieved by the Herschel–Bulkley model

$$\tau = \tau_Y + k\dot{\gamma}^n \tag{15}$$

with $\tau_Y = 7.7$ Pa, $n = 0.9$ and $k = 0.6$ Pa $s^{0.9}$, where k is the consistency index (Fig. 8a).

Fig. 8b compares the apparent viscosities of the sample before and after NaOH addition. Since the samples follow different rheologies, the coefficients representing viscosity, k and η, have different units, and so apparent viscosity μ_A is used for comparison instead. Addition of 8M NaOH increased

the apparent viscosity across all shear rates by around an order of magnitude, though the shapes of the curves themselves appear to be similar.

Geopolymerization is a complex chemical process that involves three steps: (i) alkali activation, wherein the dissolution of amorphous aluminosilicates by alkali takes place to produce monomers; (ii) reorientation, which consists of the transportation, orientation, and condensation of monomers into oligomers; and (iii) polycondensation, where the whole system hardens into an inorganic polymeric structure (Xu and Van Deventer, 2003). The viscosity increase we measured in our experiments occurs almost instantaneously and is believed to be influenced exclusively by the alkali activation step, though the higher continuous phase viscosity of the NaOH solution will also contribute. The actual hardening due to polycondensation takes longer, and usually requires several days to show an effect.

The experiments are carried out directly after the simulant is mixed with the NaOH solution in order to be consistent with the potential application of the Martian geopolymers. For construction purposes, transport of the activated slurry should occur within a short time after its preparation, and once placed, it should be left untouched for curing.

5. Design equations

In this section, the previous rheological data are converted into design tools that engineers can use in process design for the transport and storage of JSC Mars 1A slurries. Section 5.1 focus on transport, and calculates the system curve and the Moody chart for the slurries according to their concentration. Section 5.2 discusses settling that can change the properties of the slurry during storage, considering both Earth and Martian gravity.

5.1 Transport

The data gathered can be used to design equipment for handling slurries made of the dispersions discussed in this article. Engineers design piping system and pumps based on the so-called *system curve*, which provides pressure loss per length of pipe ($\Delta P/L$) as function of the flow rate (Q).

Assuming Bingham plastic rheology and using the data in Table 3 and Section 4.2, we can calculate (as discussed by Peker and Helvaci, 2007) the system curve for the cases investigated.

Figure 9a shows the system curve for various concentrations; each curve has a critical *ΔP/L* below which the pressure is not high enough to overcome the yield stress, and therefore the flow rate is zero.

Another useful tool used by engineers is the *Moody chart* that links the *Fanning friction factor f* with the Reynolds number defined as

$$Re = \frac{\rho V D}{\mu} \tag{16}$$

where ρ is the slurry density, D the diameter of the pipe, V the average velocity of the slurry, and μ the viscosity. The Fanning friction factor f, for fully developed laminar flow of a Bingham fluid in a pipe, is calculated from the implicit equation

$$f = \frac{16}{Re} + \frac{8}{3}\frac{He}{Re^2} + \frac{16}{3}\frac{1}{f^3}\frac{He^4}{Re^8} \tag{17}$$

where He is the Hedström number defined as

$$He = \frac{\rho D^2 \tau_Y}{\mu^2} \tag{18}$$

Fig. 9b shows the Moody chart for three of the dispersions investigated. The graphs of the $\phi = 0.45$ and 0.49 dispersions are almost overlapping because they have similar values of He.

For comparison, the Fanning friction factor for a Newtonian fluid (He=0) is also reported in Fig. 9b. However, we include only the laminar part of the Moody chart since transition to turbulence is not investigated in this study.

5.2 Settling

In Section 3, we mentioned that the relative density ρ_r is one of fundamental groups that affect the behaviour of the suspension, in particular influencing the settling. In Section 4, however, the effect of ρ_r was not accounted for. If settling occurs, during either transport or storage on the Martian surface,

the rheological properties of the slurry change and this must be considered at the design level along with the fact that Martian gravity is 62% lower than on Earth.

Another reason for investigating the settling concern is the rheopectic behaviour discussed in Section 4.1. Rheopexy can occur in suspensions that set slowly on standing but quickly when gently agitated (Schramm, 2014). In Section 4.1, we asserted that, in our case, rheopexy is not attributed to settling. In this section, we look closer at this assertion by investigating the settling times of the slurries.

The settling velocity of a particle in a concentrated suspension can be calculated by (Richardson et al., 2002)

$$u_P = \frac{d^2(\rho_P - \rho)g}{18\eta}(1-\phi)^{4.8} \quad (19)$$

where g is the gravity acceleration, ρ_p the density of the solid (2556 kg m^{-3}), ρ the density of the mixture (see Table 2) and η the viscosity of the mixture (see Table 3). Table 4 reports the settling velocities for the range of concentrations explored, for both the average particle size (d = 10 μm) and the maximum particle size (d = 100 μm). Results are calculated for both terrestrial and Martian gravity (9.81 and 3.71 m s^{-2} respectively). In all cases, the settling velocities are very small and unlikely to significantly affect the experiments carried out in this study. If the slurries are stored for many days, however, a certain degree of settling can occur and this should be accounted for.

6. Conclusions

The mixtures of JSC-Mars-1A with water exhibit viscoelastic behaviour and yield stresses, especially at high solid concentrations. Moreover, shear history plays a very important role in its rheology. In particular, the dispersions can be thixotropic upon rapid changes in shear-rate and rheopectic upon slower changes. On the basis of our results, we can distinguish at least five timescales that characterize the behaviour of the dispersions under stress.

1. Elastic behaviour (~0.1 s). Oscillatory tests indicate that the fluid is viscoelastic and, at small timescales, it reacts to sudden strain as an elastic solid.

2. Thixotropic behaviour (~2 s). At longer times the dispersion begins to flow, though only above a certain shear stress, since it behaves like a Bingham fluid and exhibits a yield stress. The hysteresis loops show that quick step changes (2 s duration) of shear-rate result in thixotropic behaviour.
3. Rheopectic behaviour (~10 – 100 s). The hysteresis loops for higher solids samples at slower step changes (> 10 s duration) of shear-rate show a transition from thixotropy to rheopexy.
4. Effect of ageing (~3 days). If the measurements are repeated after a few days, the rheology of the dispersion exhibits a lower yield stress.
5. Settling (~2 weeks). If the slurry is stored for long durations, settling can occur and change the rheological properties of the suspension.

In this study, the first three phenomena are explained with the breakdown and recovery of the packing structure under stress, the fourth with the stabilization of the milled surfaces and the fifth with Eq. (19).

The effect of these different timescales can have important consequences on the handling of the slurries. If the slurries are conveyed in pipes, the velocity profiles may show characteristics common to both laminar and plug flow as with Bingham fluids. These characteristics, however, will also change in both time and space. The start-up of pumps, for instance, is likely to be difficult due to yield stress and, because of the thixotropy-rheopexy transition, the slurry may exhibit a different rheology at different locations of the pipeline especially after elbows and reducers.

High solids concentrations, moreover, tend to further exacerbate these phenomena. If the slurry is stored for long times, for instance, particle settling can unexpectedly increase yield stress and cause burn-out of the pump at the start-up. Ageing, however, may partially alleviate the effect of this phenomenon since it reduces yield stress over time.

Our results show that the behaviour of mixtures of water and Martian soil simulant varies considerable form case to case and this highlights the importance of understanding the rheological characteristics of these slurries. The system curve and the Moody chart are practical outcomes of our

investigation and enable calculations for handling and transport of slurries, contributing to the groundwork of future process engineering on Mars. In situ resource utilization is the avenue for humans becoming an interplanetary species as the development of local construction materials is fundamental for realising future lunar and planetary outposts.

5. References

Alexiadis A., Alberini F., Meyer M.E., 2017. Geopolymers from lunar and Martian soil simulants, Adv. Sp. Res., 59 490–495. doi:10.1016/j.asr.2016.10.003.

Allen C.C., Jager K.M., Morris R. V., Lindstrom D.J., Lindstrom M.M., Lockwood J.P. 1998. JSC Mars-1: a Martian soil simulant, in: Sixth ASCE Spec. Conf. Expo. Eng. Constr. Oper. Sp. April 26-30, 1998, Albuquerque, New Mexico, United States, pp. 469–476. doi:10.1061/40339(206)54.

Barnes H.A., Nguyen Q.D., 2001. Rotating vane rheometry — a review, J. Non-Newtonian Fluid Mech. 98, 1–14. doi:10.1016/S0377-0257(01)00095-7.

Barnes H.A., Walters K., 1985. The yield stress myth?, Rheol. Acta. 24, 323–326. doi:10.1007/BF01333960.

Brown E., Jaeger H.M., 2012. The role of dilation and confining stresses in shear thickening of dense suspensions, J. Rheol. (N. Y. N. Y). 56, 875–923. doi:10.1122/1.4709423.

Cesaretti G., Dini E., De Kestelier X., Colla V., Pambaguian L., 2014. Building components for an outpost on the Lunar soil by means of a novel 3D printing technology, Acta Astronaut. 93, 430–450. doi:10.1016/j.actaastro.2013.07.034.

Chappuis J., Guinot D., Leture P., 1992. Rheological Properties of Dense Silica Suspensions, Mater. Res. Soc. Symp. Proc. 289, 87–94. doi:10.1557/PROC-289-87.

Cheng D.C.H., Richmond R.A., 1978. Some observations on the rheological behaviour of dense suspensions, Rheol. Acta. 17, 446–453. doi:10.1007/BF01525960.

Cheng D.C.H., 1984. Further observations on the rheological behaviour of dense suspensions, Powder Technol. 37, 255–273. doi:10.1016/0032-5910(84)80022-4.

Cheng X., McCoy J.H., Israelachvili J.N., Cohen I., 2011. Imaging the Microscopic Structure of Shear Thinning and Thickening Colloidal Suspensions, Science 333, 1276–1279. doi:10.1126/science.1207032.

Duran J., 2000. Sands, powders, and grains : an introduction to the physics of granular materials, Springer Science, London, doi:10.1007/978-1-4612-0499-2.

Fall A., Huang N., Bertrand F., Ovarlez G., Bonn D., 2008. Shear thickening of cornstarch suspensions as a reentrant jamming transition, Phys. Rev. Lett. 100, 18301. doi:10.1103/PhysRevLett.100.018301.

Happel J.A., 1993. Indigenous Materials for Lunar Construction, Appl. Mech. Rev. 46, 313–325. doi:10.1115/1.3120360.

Kawasaki T., Ikeda A., Berthier L., 2014. Thinning or thickening? Multiple rheological regimes in dense suspensions of soft particles, Europhys. Lett. 107, 1–6. doi:10.1209/0295-5075/107/28009.

Lin W., Wendner R., Cusatis G., 2016. A novel material for in situ construction on Mars: experiments and numerical simulations, Construction and Building Materials 120, 222–231.

Leach N., Carlson A., Khoshnevis B. Thangavelu M., 2012. Robotic Construction by Contour Crafting: The Case of Lunar Construction International Journal of Architectural Computing 10, 423-438.

Montes C., Broussard K., Gongre M., Simicevic N., Mejia J., Tham J., Allouche E., Davis G., 2015. Evaluation of lunar regolith geopolymer binder as a radioactive shielding material for space exploration applications, Adv. Sp. Res. 56, 1212–1221. doi:10.1016/j.asr.2015.05.044.

Mukbaniani O. V., Aneli J.N., Markarashvili E.G., Tarasashvili M. V., Aleksidze N.D., 2015. Polymeric composites on the basis of Martian ground for building future mars stations, Int. J. Astrobiol. 15, 1–6. doi:10.1017/S1473550415000270.

Ness C., Sun J., 2016. Shear thickening regimes of dense non-Brownian suspensions, Soft Matter. 12, 914–924. doi:10.1039/c5sm02326b.

Ovarlez G., 2011. Introduction to the rheometry of complex suspensions, in: N. Roussel (Ed.), Underst. Rheol. Concr., Woodhead Publishing. doi:10.1533/9780857095282.1.23.

Peker S., Helvaci S., 2007. Solid-Liquid Two Phase Flow, 1st ed., Elsevier Science.

Quemada D., 1985. Phenomenological rheology of concentrated dispersions. I. Clustering effects and the structure-dependent packing fraction, J. Mec. Theor. Appl., 267–288.

Richardson J.F., Harker J.H., Backhurst J.R., 2002. Chemical Engineering, 5th ed., Springer.

Saak A.W., Jennings H.M., Shah S.P., 2001. The influence of wall slip on yield stress and viscoelastic measurements of cement paste, Cem. Concr. Res. 31, 205–212. doi:10.1016/S0008-8846(00)00440-3.

Schramm G. 1994, A Practical Approach to Rheology and Rheometry, Gebrueder Haake.

Schramm L.L., 2014. Emulsions, Foams, Suspensions, and Aerosols: Microscience and Applications, 2nd ed., Wiley VCH.

Stickel J.J., Powell R.L., 2005. Fluid Mechanics and Rheology of Dense Suspensions, Annu. Rev. Fluid Mech. 37, 129–149. doi:10.1146/annurev.fluid.36.050802.122132.

Taylor S.R., McLennan S., 2008. Planetary Crusts: Their Composition, Origin and Evolution, Cambridge University Press.

Wagner N., Brady J., 2009. Shear thickening in colloidal dispersions, Phys. Today. 62, 27–32. doi:10.1063/1.3248476.

Xu H., Van Deventer J.S.J., 2003. Effect of Source Materials on Geopolymerization, Ind. Eng. Chem. Res. 42, 1698–1706. doi:10.1021/ie0206958.

TABLES

Oxide [wt%]	Martian Simulant JSC Mars-1A	Martian Regolith
SiO_2	43.7	45.41
TiO_2	3.8	0.91
Al_2O_3	23.4	9.70
Fe_2O_3	11.8	-
FeO	3.5	16.73
MgO	3.4	8.35
CaO	6.2	6.37
Na_2O	2.4	2.73
SO_3	-	6.16

Table 1. Comparison of elemental oxide compositions of JSC-Mars-1 (Allen et al., 1998), and the average Martian regolith composition (Taylor and McLennan, 2008).

Dry solids [g]	Total water [g]	Solids content [wt%]	Volume fraction ϕ [-]	Density ρ [kg m^{-3}]
50	20	71.4	0.49	1769
50	21	70.4	0.48	1750
50	22	69.4	0.47	1732
50	23.5	68.0	0.45	1706
50	25	66.7	0.44	1685
50	27	64.9	0.42	1652
50	31	61.7	0.39	1601

Table 2. Composition of the samples investigated

ϕ [-]	τ_Y [Pa]	η [Pa s]	α [Pa s^{-1}]
0.49	68	0.29	-1047
0.48	48	0.22	-116
0.47	33	0.16	-8.0
0.45	20	0.12	95
0.44	8.6	0.09	74
0.42	2.3	0.06	52
0.39	0.5	0.03	34

Table 3. Effect of solids content on selected rheological properties.

ϕ [-]	u^T_p (10 µm) [mm hr^{-1}]	u^T_p (100 µm) [cm hr^{-1}]	u^M_p (10 µm) [mm hr^{-1}]	u^M_p (100 µm) [cm hr^{-1}]
0.49	0.02	0.20	0.01	0.08
0.48	0.03	0.31	0.01	0.12
0.47	0.05	0.48	0.02	0.18
0.45	0.08	0.76	0.03	0.29
0.44	0.12	1.18	0.04	0.45
0.42	0.22	2.16	0.08	0.82
0.39	0.60	5.96	0.23	2.26

Table 4. Settling velocity for the average particles size (10 µm) and the maximum size (100 µm): u^T_P is the settling velocity based on terrestrial gravity, u^M_P is the settling velocity based on Martian gravity.

FIGURES

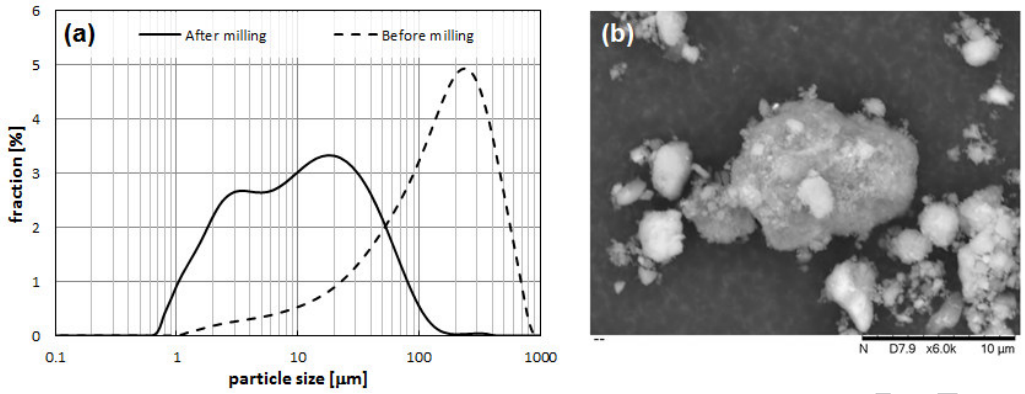

Figure 1. Particle size distribution before and after milling (a), SEM image of the milled JSC MARS-1A (b)

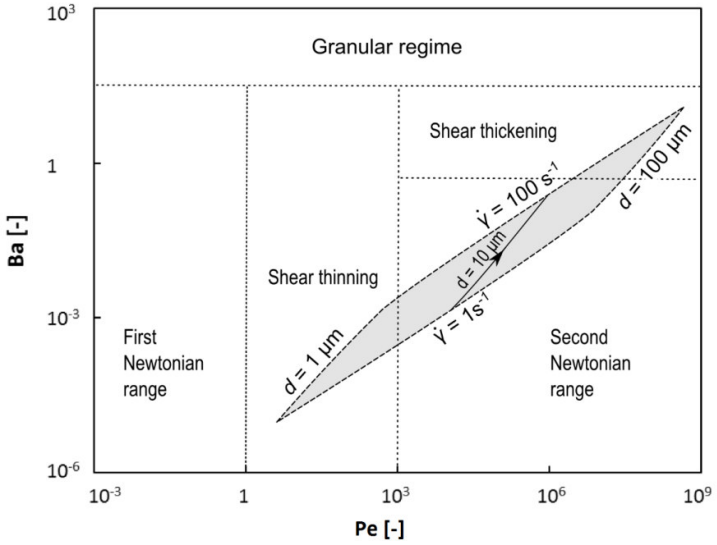

Figure 2. Schematic 'phase diagram' of dispersion rheology

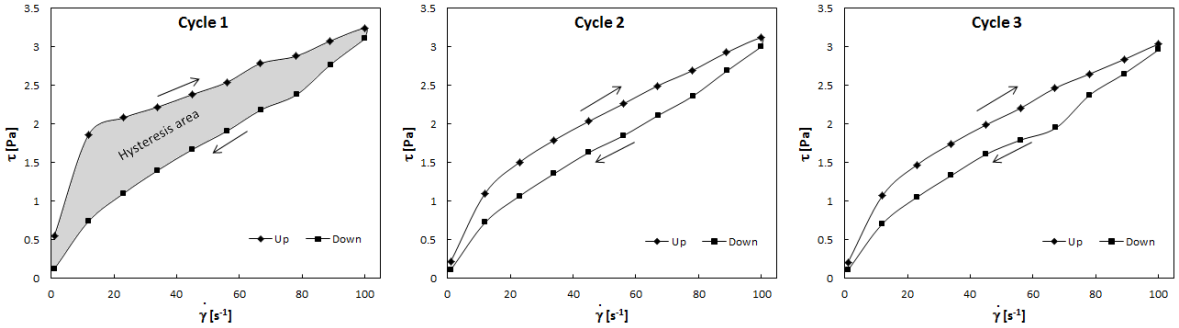

Figure 3. First three hysteresis loops for the $\phi = 0.39$ sample, with 2 s step durations.

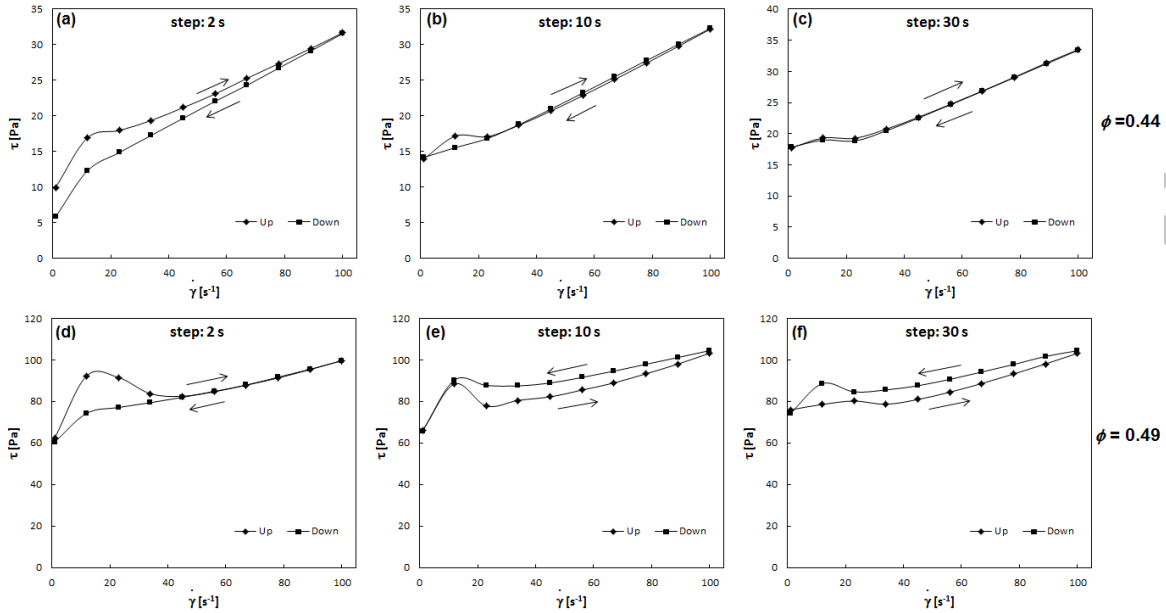

Figure 4. Equilibrium hysteresis loops at various step durations (2 s, 10 s and 30 s) and solid contents.

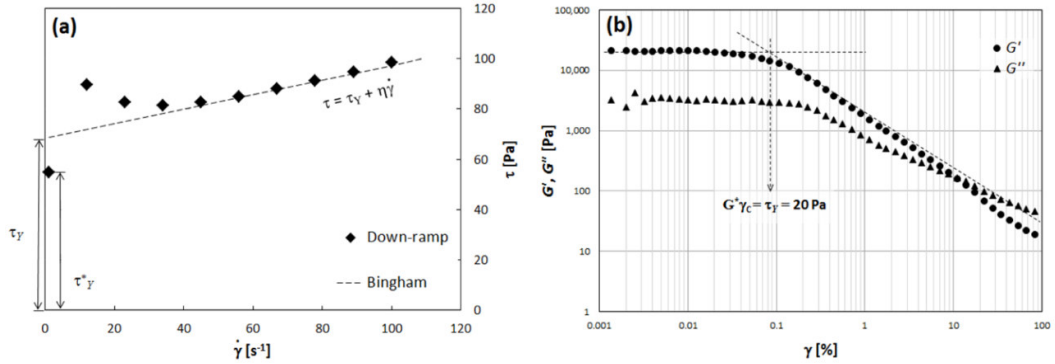

Figure 5. Bingham fitting (a) and oscillatory test (b) for the ϕ= 0.49 dispersion

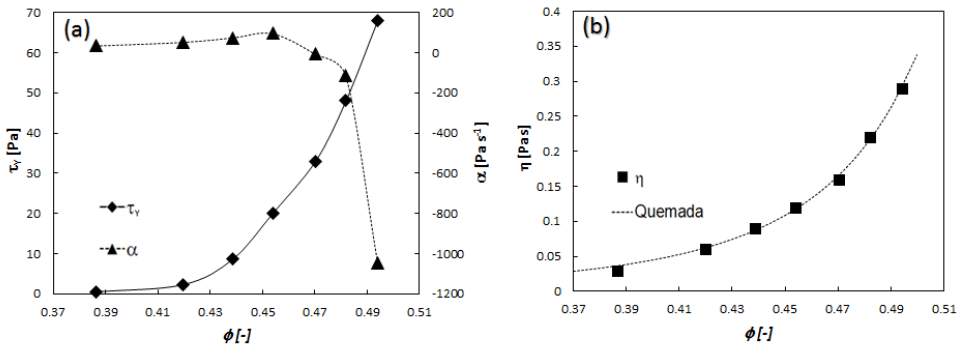

Figure 6. Effect of solids volume fraction ϕ on yield stress τ_Y and the 10 s duration hysteresis area α (a), comparison between the Bingham viscosity η and the generalized Quemada equation (b).

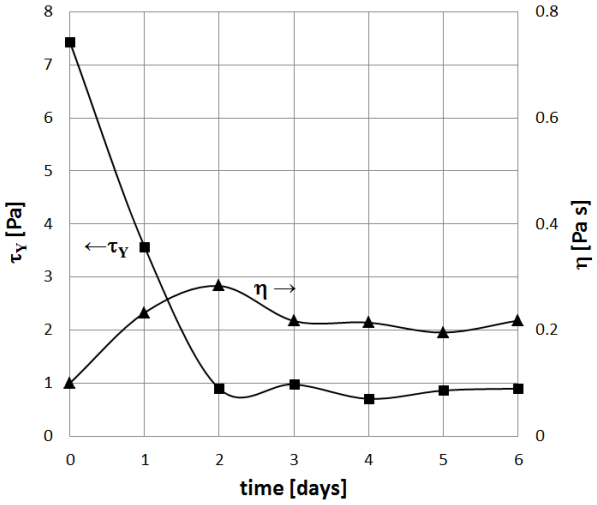

Figure 7. Effect of ageing in the $\phi = 0.44$ dispersion.

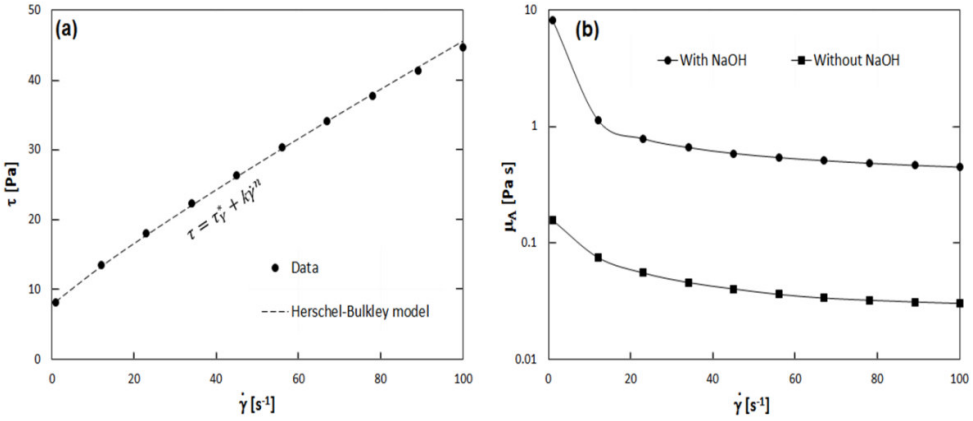

Figure 8. Flow curve for the $\phi = 0.39$ sample after the addition of 8M NaOH (a), comparison of the apparent viscosity with the untreated sample (b).

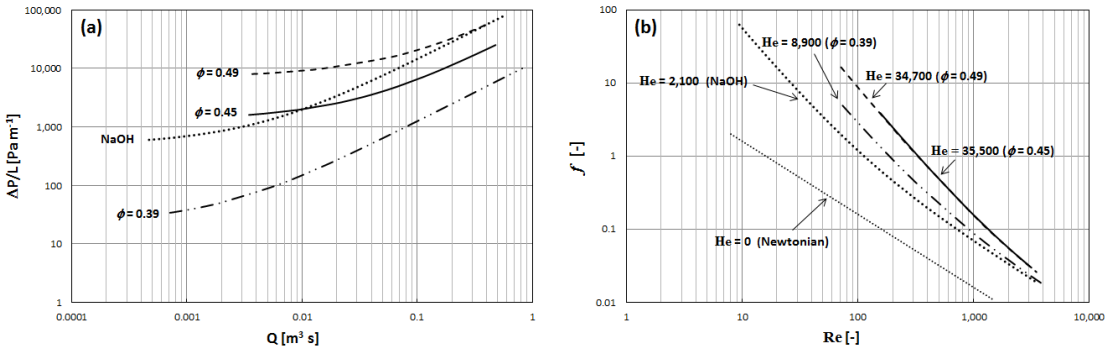

Figure 9 System curve (a) and Moody Chart with Fanning friction factor (b) for various slurry concentrations.

Highlights

Alkaline suspensions of Martian soil simulant form geopolymers for building purposes

In-situ production of geopolymers will necessitate handling Martian-soil slurries

The rheology of slurries of water and JSC-Mars-1A is investigated

Designing tools that engineers on Mars could use for slurry equipment are given